



HAL
open science

Whistlers observed by the Cluster spacecraft outside the plasmasphere.

M. Platino, U.S. Inan, T.F. Bell, D.A. Gurnett, J.S. Pickett, P. Canu,
Pierrette Décréau

► **To cite this version:**

M. Platino, U.S. Inan, T.F. Bell, D.A. Gurnett, J.S. Pickett, et al.. Whistlers observed by the Cluster spacecraft outside the plasmasphere.. *Journal of Geophysical Research Space Physics*, 2005, 110 (A3), pp.A03212. 10.1029/2004JA010730 . hal-00153623

HAL Id: hal-00153623

<https://hal.science/hal-00153623>

Submitted on 29 Jan 2016

HAL is a multi-disciplinary open access archive for the deposit and dissemination of scientific research documents, whether they are published or not. The documents may come from teaching and research institutions in France or abroad, or from public or private research centers.

L'archive ouverte pluridisciplinaire **HAL**, est destinée au dépôt et à la diffusion de documents scientifiques de niveau recherche, publiés ou non, émanant des établissements d'enseignement et de recherche français ou étrangers, des laboratoires publics ou privés.

Whistlers observed by the Cluster spacecraft outside the plasmasphere

M. Platino,¹ U. S. Inan,¹ T. F. Bell,¹ D. A. Gurnett,² J. S. Pickett,²
P. Canu,³ and P. M. E. Décréau⁴

Received 9 August 2004; revised 4 December 2004; accepted 6 January 2005; published 15 March 2005.

[1] Lightning generated whistlers are ubiquitous within the plasmasphere at both high and low altitudes, and these waves propagate efficiently in both ducted and nonducted modes. On the other hand, in the magnetospheric region outside the plasmasphere, lightning-generated whistlers are commonly observed at low altitudes (up to ~ 6000 km) but only rarely at higher altitudes near the magnetic equatorial plane. The reasons for the lack of these waves at higher altitudes are not well understood. In the present paper we use data from the Wide Band Plasma (WBD) instruments on the four Cluster spacecraft to study the characteristics of lightning-generated whistlers observed on 4 separate days in 2001 at L shells ranging from $L = 4$ to $L = 5$, magnetic latitudes ranging from -20° to 10° , and Kp indices ranging from 3 to 6. The propagation paths of the lightning-generated whistlers are determined using a two-dimensional ray-tracing model to calculate the ray paths and group delays from the lower ionosphere to each of the four Cluster spacecraft over a range of frequencies ($1 \text{ kHz} < f < 8 \text{ kHz}$). The electron density distributions used for the ray-tracing calculations are derived from measurements with the Whisper relaxation sounder instrument. Our new results indicate that whistlers are observed outside the plasmasphere in the low-density regions only in the presence of large-scale irregularities within which the waves are “ducted.” This conclusion is sustained by an exhaustive search of whistlers outside the plasmasphere using all the Cluster passes during 2001 and 2002. In all the cases we found that dispersion characteristics are matched by ray-tracing simulations only if the whistlers are ducted. In some cases, whistler wave energy injected by an individual lightning discharge appears with significant smearing in time. The new results presented in this paper support a possible explanation of why whistlers outside the plasmasphere are rarely observed, based on wave conversion electromagnetic whistler mode to quasi-electrostatic lower hybrid mode (Bell et al., 2004).

Citation: Platino, M., U. S. Inan, T. F. Bell, D. A. Gurnett, J. S. Pickett, P. Canu, and P. M. E. Décréau (2005), Whistlers observed by the Cluster spacecraft outside the plasmasphere, *J. Geophys. Res.*, *110*, A03212, doi:10.1029/2004JA010730.

1. Introduction

[2] The propagation of whistlers in ducts of enhanced ionization was first investigated by Smith [1961] and is extensively discussed by Helliwell [1965]. Angerami [1970] reported the first direct evidence on the nature of ducts, based on in situ whistler observations on board the OGO 3 satellite. Analysis of OGO 3 spacecraft data yielded several physical characteristics of the ducts observed, experimental confirmation of predicted properties of ducted propagation [Angerami and Carpenter, 1966; Angerami, 1966], evi-

dence of diffusive equilibrium type of field line distribution of ionization in the plasmasphere, and validation of the results of ray-tracing simulations [Cerisier, 1967]. The sharp boundary of the plasmopause is also known to be an effective guide for VLF whistler mode energy with larger-density gradients leading to increased guidance efficiency [Inan and Bell, 1977].

[3] In the present work we focus on observations of whistlers on the Cluster spacecraft when they are clearly outside the plasmasphere. (i.e., at L shells values at the observation points which are higher than that corresponding to the location of the plasmopause).

[4] Previous reports of whistlers propagating outside the plasmasphere [Carpenter and Šulić, 1988] and near the plasmopause [Carpenter, 1978] have been reported based on ground measurements. These reports show features such as VLF noise bands and bursts triggered by the whistlers, which travel along local enhancements or depletions of plasma density referred as “ducts” or “troughs,” respectively, together with the triggering whistler wave, in a similar fashion as those reported in the present paper.

¹STAR Laboratory, Stanford University, Stanford, California, USA.

²Department of Physics and Astronomy, University of Iowa, Iowa City, Iowa, USA.

³Centre d'Études des Environnements Terrestres et Planétaires, Centre National de la Recherche Scientifique, Université Versailles Saint-Quentin-en-Yvelines, Vélizy Villacoublay, France.

⁴Laboratoire de Physique et Chimie de l'Environnement, Centre National de la Recherche Scientifique, Orléans, France.

Carpenter and Šulić [1988] established that ducted whistler propagation outside the plasmasphere occurs relatively rarely, compared with the whistler occurrence within the boundaries of the plasmapause. It was also established that ground detection of whistler waves generally occur at localized regions of the magnetosphere and that the amplitudes of such whistlers are on average lower than those observed in the plasmasphere. This fact was originally noted based on in situ observations on the Alouette 1 and 2 spacecraft [*Carpenter et al.*, 1968] and the OGO1 and OGO 3 spacecraft [*Carpenter et al.*, 1969], where a strong reduction was observed of the occurrence of lightning-generated whistlers and VLF noise (plasmaspheric hiss) upon crossing the plasmapause (within a distance of ~ 100 km).

[5] Data shown in this paper were acquired during 2001 and 2002, with the Wide Band Plasma Instruments [*Gurnett et al.*, 1997] on the Cluster spacecraft. All calculations are based on simultaneous observations of electron densities on the same spacecraft, using the Whisper instrument [*Décrou et al.*, 1997].

[6] From the data studied, four cases were chosen to be modeled with ray tracing. The objective of ray-tracing calculations is to show that propagation times and dispersion properties for different frequencies allow the reconstruction of whistler waves observed in regions where the plasma density is highly irregular, as is commonly found to be the case for the cases studies herein.

2. Cluster and the WBD Instrument

[7] The Cluster orbit crosses many regions of scientific interest during the course of the mission. When the apogee is around local noon, the regions successively crossed are the nightside auroral zone, the northern cusp, the magnetopause, the bow shock, the solar wind, and then again the same regions in the Southern Hemisphere. Special emphasis in terms of separation has been put on the northern cusp and tail crossings at 17–19 R_e . In these two areas a perfect tetrahedron has been constituted. Near perigee, the configuration becomes elongated and the spacecraft cross the auroral zone as a “string of pearls.” The interspacecraft separations have been varied between 100 and 5000 km.

[8] The Cluster Wide Band (WBD) Plasma Wave Investigation [*Gurnett et al.*, 1997] is designed to provide very high-resolution frequency-time measurements of plasma waves in the Earth’s magnetosphere. The WBD instrument consists of a digital wideband receiver that can provide electric or magnetic field waveforms over a wide range of frequencies. The wideband technique involves transmitting band-limited waveforms directly to the ground using a high-rate data link. The primary advantage of this approach is that continuous waveforms are available for detailed high-resolution frequency-time analysis. The wideband technique has the advantage that the resolution can be adjusted to provide optimum analysis of the phenomena of interest.

3. Ray-Tracing Technique

[9] The ray-tracing technique presented in this paper was originally developed by *Haselgrove* [1954] and *Yabroff* [1961]. This technique was implemented in a computer

program [*Kimura*, 1966] and further developed into the actual version used for the computations presented here. We use a geomagnetic field model based on a centered dipole with electron gyrofrequency of 880 kHz at the ground on the magnetic equator. The electron and ion densities above 1000 km and below the plasmapause (where densities are above 10^2 el/cm^3) are represented by a field-aligned isothermal ($T=1600^\circ\text{K}$) diffusive equilibrium model [*Angerami and Carpenter*, 1966]. In all cases considered, the compositions at 1000 km altitude is taken to be 90% O^+ , 8% H^+ , and 2% He^+ . Outside the plasmasphere, the model used is an approximation of the collisionless model, called the R^{-4} model, which, as described by *Angerami and Carpenter* [1966], is more suitable for this region.

[10] The initial density of electrons at 1000 km was chosen in accordance with the diffusive equilibrium model to fit the density profile deduced on the basis of data from the Whisper resonance sounder [*Décrou et al.*, 1997]. The Whisper sounder on the Cluster spacecraft is primarily designed to provide an absolute measurement of the total plasma density N_o within the range 0.2–80/ cm^3 . This measurement is achieved by means of a resonance sounding technique, which has already proved successful in the regions to be explored [*Etcheto et al.*, 1983; *Trotignon et al.*, 1986]. The wave analysis function of the instrument is provided by Fast Fourier Transform (FFT) calculation. In the basic nominal operational mode, the density is measured by the sounder every 52 s. In the time interval between sounder operations, Whisper operates in the so-called Natural wave mode. Frequency-time measurements of natural electric fluctuations are acquired at a frequency and time resolution of about 320 Hz and 2.2 s, respectively.

[11] Figure 1 shows representative frequency-time spectrograms generated from measured data using Whisper in its Natural wave operational mode. The three panels show spectrograms of the electric field along the z axis (i.e., along one of the spin axis booms) for the three dates studied. Figure 1a shows a measurement of the \mathbf{E}_z field on spacecraft SC3 on 24 April 2001. Figure 1b shows a measurement of the \mathbf{E}_z field on spacecraft SC1 on 20 June 2001. Figure 1c shows a measurement of the \mathbf{E}_z field on spacecraft SC1 on 21 July 2001.

[12] The Whisper sounding technique is based on the identification of the electron plasma frequency by analyzing the pattern of resonances triggered in the medium by a pulse transmitter [*Trotignon et al.*, 2001]. The plasma resonances, which are characterized by low group velocity and which can be triggered, are the electron plasma frequency, the electron gyrofrequency, the upper hybrid frequency, and other Bernstein waves [*Bernstein*, 1958]. Once clearly identified by the sounder, the characteristic plasma frequencies marked by resonances can be followed in the frequency-time spectral intensities of natural emissions measured by Whisper [*Canu et al.*, 2001]. In particular, we currently see banded emissions between the electron plasma frequency and the upper hybrid resonance frequency (see for instance Figure 1c, the 41–43 kHz band at 0234 UT).

[13] By using a combination of active (in Sounding mode) and passive (in Natural wave mode) Whisper measurements, the electron density is derived as a function of the spacecraft position. The measured data are then projected to the magnetic equator, assuming that the electron density profile varies

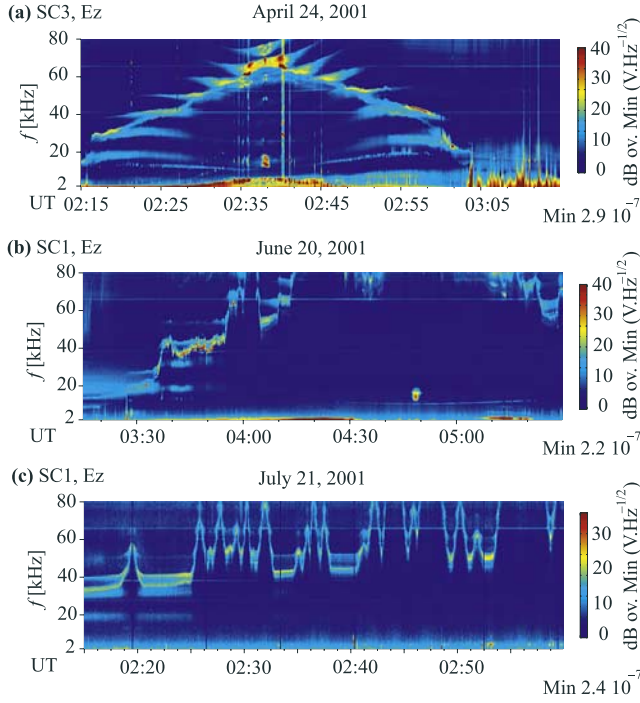


Figure 1. Whisper sounder electric field spectrograms for the three dates studied. The spectrograms show the magnitude of the electric field. These three different days show a variety of electron density structures, from a very compressed plasmasphere on the first panel where the plasma is smoother to more irregular plasma on the third panel. (a) Data recorded on 24 April 2001. (b) Data recorded on 20 June 2001. (c) Data recorded on 21 July 2001.

as R^{-4} , where R is the radial distance from the Earth. These projections are used to build an equatorial density profile over the L shell range for which $N_o \leq 80 \text{ el/cm}^3$. For regions in which $N_o > 80 \text{ el/cm}^3$, we use the model of *Carpenter and Anderson* [1992] to complete our density profile at lower altitudes (i.e., $R < 4$) where we do not have Whisper data available. The use of this model is necessary since some of the ray paths start out from L shells for which $N_o > 80 \text{ el/cm}^3$. It is important to notice that the electron density model proposed by *Carpenter and Anderson* [1992] depends on the maximum Kp index of the previous 24 hours and therefore does not reflect the actual density profile in detail but rather represents an average of it. Being based on an average Kp , we must use some other source of information to determine the actual electron density at the spacecraft and corroborate the calculations with the actual value of electron density. In order to do this, we derive the electron density and the L shell of propagation of the whistlers analyzed, using the whistler dispersion analysis method described by *Park* [1972]. The use of the whistler dispersion analysis implies an assumption that the whistler waves are “ducted.” Why this is so is not obvious in general since nonducted signals are much more commonly observed at spacecraft; the results of our analysis in this paper do indeed suggest that the whistlers observed on the Cluster spacecraft propagate within large-scale field-aligned irregularities so that their dispersion properties closely resemble those of ducted whistlers.

[14] The *Park* [1972] method consists of using the R^{-4} model to infer the electron density from the nose frequency of the whistler in a five-step procedure.

[15] 1. Measure the nose frequency f_n from the data and estimate the propagation delay at the nose frequency, t_n , using ray tracing. Table 1 shows the measured values of f_n and t_n used in all four cases analyzed.

[16] 2. Decide on a magnetospheric electron concentration model to be used. In our case, we used the already specified diffusive equilibrium model, with a composition of 90% O⁺, 8% H⁺, and 2% He⁺, at 1000 km of altitude, in a plasma temperature of 1600°K, for propagation inside the plasmasphere and the R^{-4} model for propagation outside the plasmasphere. Since the spacecraft were moving outside the plasmasphere during the passes we studied, we use the R^{-4} model for the calculations in Table 1.

[17] 3. Estimate the dispersion in the ionosphere, D_{ci} , corresponding to the path the wave travels along the Earth-ionosphere waveguide until it leaks out into space. This parameter depends on the electron density in the ionosphere; particularly, it can be approximated as $D_{ci} = 0.7 f_{oF2}$, where f_{oF2} is the F2 layer cutoff frequency in MHz. Since the expressions used to calculate this correction are not significantly sensitive to D_{ci} , we assumed the same value for it in all four cases analyzed, of $D_{ci} = 2.5$.

[18] 4. Make the corrections for the ionospheric dispersion to obtain f'_n and t'_n as follows (These are formulas for the R^{-4} model):

$$f'_n = \frac{f_n}{1 + \left[\frac{0.15 \cdot D_{ci}}{t_n \cdot f_n^{1/3}} \right]}, \quad t'_n = t_n - D_{ci} \cdot \left(\frac{f_n + f'_n}{2} \right)^{-1/2}, \quad (1)$$

where t_n and t'_n are in seconds and f_n and f'_n are in Hz. The calculated values of these parameters are summarized in Table 1.

[19] 5. The L shell values and the projected electron density to the equator, N_o , are calculated from the following empirical formulas:

$$f_{Heq} = K \cdot f'_n L = \left(\frac{8.736 \cdot 10^5}{f_{Heq}} \right)^{1/3} N_o = K_{eq} \cdot \frac{f'_n \cdot t'^2_n}{L^5}. \quad (2)$$

In these formulas, N_o represents the value of electron density projected to the magnetic equator ($0^\circ \lambda_m$), along the L shell of the spacecraft. The values of K and K_{eq} are

Table 1. Results From the Calculations for N_o and L From the Nose Frequencies of the Whistlers Studied^a

	04/24/2001 0218:38 UT	06/20/2001 0514:09 UT	06/20/2001 0521:30 UT	07/21/2001 0248:28 UT
D_{ci}	2.5	2.5	2.5	2.5
t_n , s	0.28	0.28	0.29	0.8
f_n , Hz	4,900	4,700	4,700	2,800
f'_n , Hz	4,500	4,310	4,320	2,700
t'_n , s	0.24	0.24	0.25	0.75
K	2.29	2.29	2.29	2.26
f_{Heq} , Hz	10,300	9,900	9,900	6,100
L	4.15	4.2	4.2	4.9
K_{eq}	7.9	7.9	7.9	7.6
N_o , cm^{-3}	1.7	1.5	1.65	4.08

^aThese values of N_o were used to compare with the plasma densities shown in Figure 3. All the intermediate parameters were used for the calculations, as described by *Park* [1972].

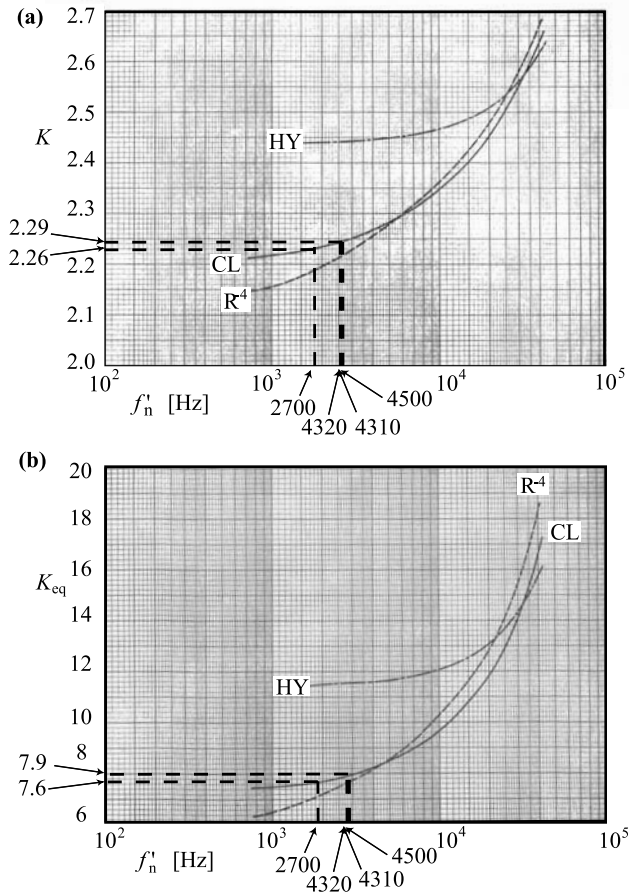


Figure 2. Values of parameters (a) K and (b) K_{eq} , used to calculate the L and N_0 for the four cases studied. The three curves in each panel correspond to different models that can be used to calculate the electron density of the plasma in the region outside the plasmasphere: *CL*: the collisionless model; *HY*: the hybrid model; R^{-4} : an approximation of the collisionless model called the R^{-4} model.

calculated from the curves on Figure 2. These curves were generated by *Park* [1972] and show the variation of K and K_{eq} for different plasma density models, as a function of the corrected frequency f_n . The model we use corresponds to the curve R^{-4} in Figures 2a and 2b. The results of these calculations are summarized in Table 1. The values of L shell and N_0 were used to corroborate the plasma density values obtained from *Whisper* and to determine whether the dipole model provides an appropriate fit to the actual configuration of the Earth's magnetic field.

[20] Figure 3 shows the resulting density profiles at the equator for the 3 days. The three panels shown in Figure 3 reflect the values of electron density extracted from *Whisper* profile obtained from the *Carpenter and Anderson* [1992] model. The irregularities in the electron density profile are assumed to be field-aligned enhancements of ionization and are included in the code by multiplying the densities given by the R^{-4} model, with a product of bell-shaped functions for each enhancement:

$$N_0 = N_{DE} \cdot \prod_{i=1}^m \left\{ 1 + C_i \cdot \exp\left(\frac{-(L - L_i)^2}{2 \cdot \Delta L_i^2}\right) \right\}, \quad (3)$$

where

- N_0 plasma electron density at the equator;
- N_{DE} plasma electron density derived from model;
- m number of enhancements;
- C_i enhancement at i th duct;
- L local L shell;
- L_i L shell at center of i th duct;
- ΔL_i semiwidth of i th duct.

[21] Using the *Carpenter and Anderson* [1992] model as a baseline, following the measured densities obtained from *Whisper*, enhancements were added for each case, with the

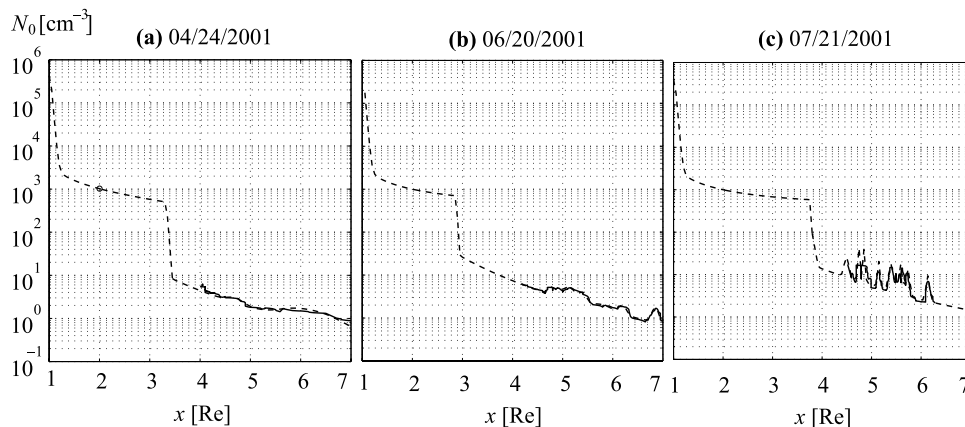


Figure 3. Electron density profiles reconstructed from the *Whisper* electric field measurements for the three dates studied. These are constructed from direct measurement of the plasma frequency using *Whisper* data at different magnetic latitudes and then projected to the equator, assuming an R^{-4} variation of the electron density with radial distance from the Earth. (a) Profile for 24 April 2001; the full curve is the electron density measured, while the dashed curve is the model. (b) Profile for 20 June 2001; the full curve is the electron density measured, while the dashed curve is the model. (c) Profile for 21 July 2001; the full curve is the electron density measured, while the dashed curve is the model.

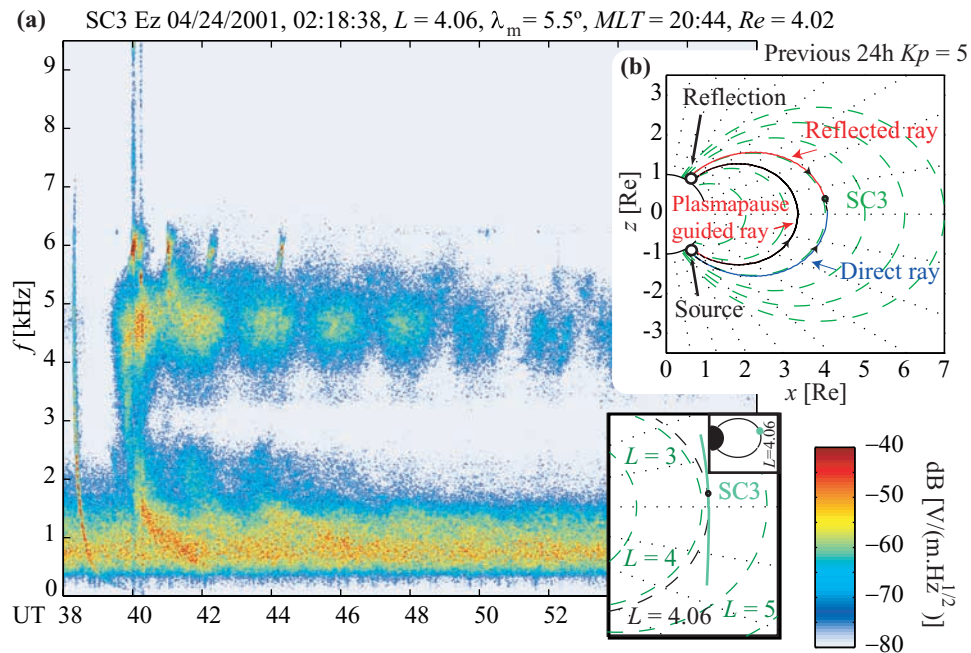


Figure 4. (a) WBD electric field spectrogram for 04/24/2001 when whistlers outside the plasmasphere were recorded. Displayed are time, location of the spacecraft, and geomagnetic activity index Kp . This figure shows a whistler and its reflection, along with some triggered emissions. There were data available only for one spacecraft during this pass. (b) Modeled situation that explains the behavior of the observed whistler. A wave is launched in the Southern Hemisphere and it is guided through the plasmapause to the conjugate point, where it is reflected back to the spacecraft. Another ray reaches the spacecraft following a direct path from the Southern Hemisphere.

coefficients C_i , L_i , and ΔL_i chosen accordingly to fit the Whisper data projected to the magnetic equator.

[22] The density profiles constructed in this manner are then used as inputs for the ray-tracing code. The smooth solid line represents the calculations based on the *Carpenter and Anderson* [1992] model. Superimposed on top are the values of electron density, obtained from the Whisper instrument, as projected to the equator. The derived density profiles for 24 April 2001, 20 June 2001, and 21 July 2001 are shown in Figures 3a, 3b, and 3c, respectively. The maximum Kp indexes for the 3 days in the previous 24 hours, used in the Carpenter and Anderson model, are as follows:

04/24/2001 – max $Kp = 5$

06/20/2001 – max $Kp = 6$

07/21/2001 – max $Kp = 4$.

4. Observations: Whistlers Recorded Outside the Plasmasphere

[23] Wideband data with the WBD instrument is typically acquired for no more than 2 hours a day. Of this data, typically less than 1% is acquired near the perigee, where Cluster spacecraft are at L shells in the vicinity of the

plasmasphere. Examination of all the Cluster WBD data available for the years 2001 and 2002 indicated very few cases of whistlers observed outside the plasmasphere. Examples of all the cases of whistlers observed from January 2001 to June 2002 are displayed in this paper, in the form of frequency-time spectrograms as shown in Figures 4 to 11. An important feature of the data is the fact that very few whistlers were observed during each pass. Another important detail to notice is that the Kp indices for each day are relatively high, usually above or equal to 4, suggesting that high magnetic activity is a common characteristic of all the cases. Figures 4, 5, 6, and 7 show spectrograms of whistlers recorded by the WBD instrument outside the plasmasphere during 2001. Figures 8, 9, 10, and 11 show spectrograms of whistlers recorded by the WBD instrument outside the plasmasphere during 2002. We also show in Figures 4 to 11 selected examples from seven different passes, constituting all of the perigee passes for which data were recorded from January 2001 to June 2002. In the data from these seven passes, we found a total of 35 whistler events consisting of either a single hop or multiple hops (reflected). On dates such as 2 August 2001, no more than two whistlers are detected in the entire pass, while on dates such as 23 April 2002, up to eight whistlers are detected along a similar trajectory. From these measurements, four cases were picked for analysis and are displayed in Figures 4, 5, 6, and 7, as described in the previous section. The criteria used in selecting these cases were the clarity of the intensity of the whistlers and the diversity in structure of the electron density profiles in

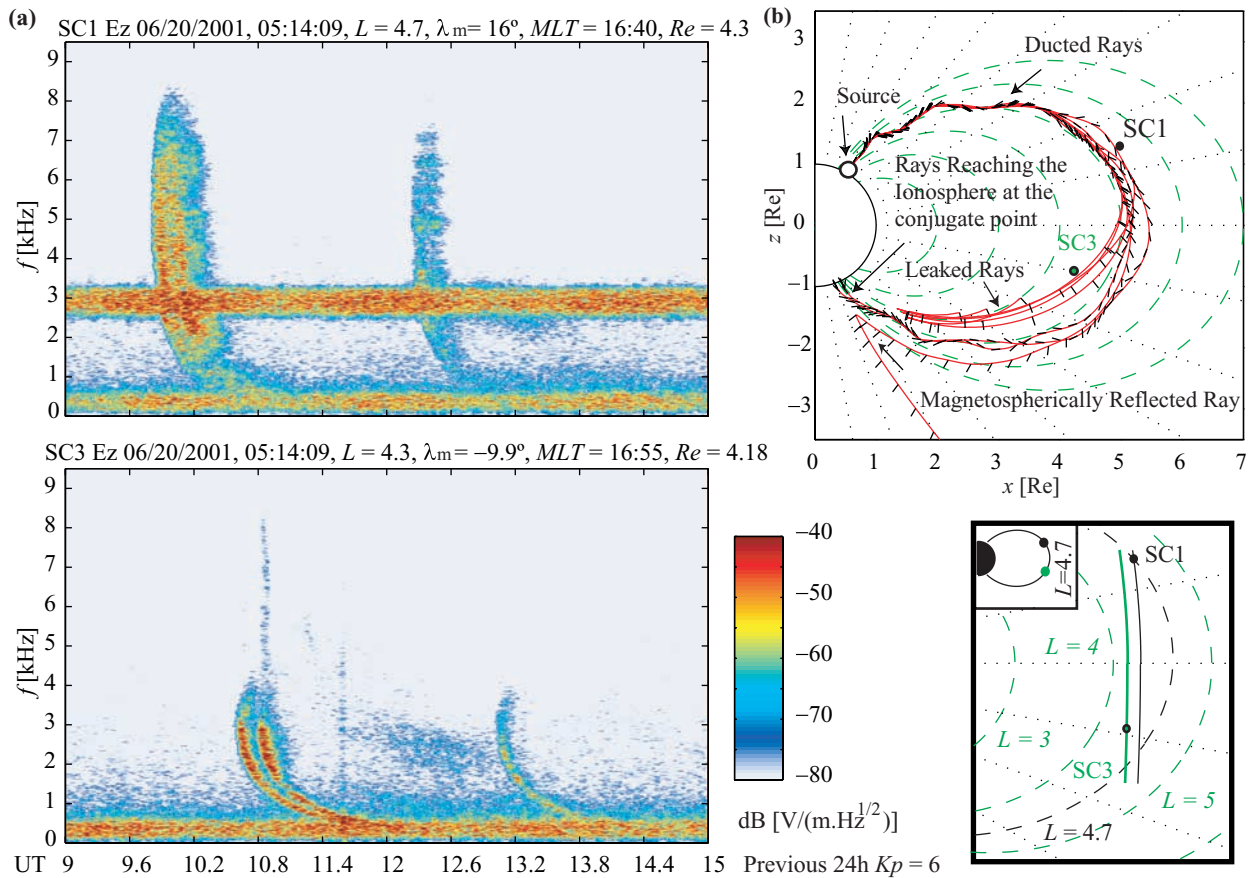


Figure 5. (a) WBD electric field spectrogram for 06/20/2001, when whistlers outside the plasmasphere were recorded. Displayed are time, location of the spacecraft, and geomagnetic activity index Kp . We find two whistlers detected on two different spacecraft, with different dispersion characteristics, due to the separation of spacecraft SC1 and SC3 in latitude. (b) Modeled situation that explains how we see the same whistler on spacecraft SC1 and SC3, being on different L shells. The whistler we see in SC3 is likely leaked from the duct at $L \sim 5$.

associated Whisper data. As we see from Figures 4 to 7, the cases selected range from a highly irregular plasma profile beyond $L = 4$ (for 07/21/2001) to a much smoother density variation (for 04/24/2001). The separation between some of the spacecraft during 2001 (displayed in Figures 5 and 6a) was very large, ~ 7600 km. As the year progressed the Cluster spacecraft were placed closer together, ~ 1300 km and ~ 800 km (as displayed in Figures 6b and 7a, respectively). The separation between the spacecraft during 2002 was significantly reduced to ~ 600 km (see Figures 9, 10, and 11), except on 01/15/2002 (Figure 8) where the separation was ~ 7900 km.

5. Data Recorded During 2001

[24] Figure 4a shows a whistler, reaching the SC3 spacecraft at 0218:38.35 UT on 04/24/2001, exhibiting a nose frequency of 4.9 kHz. According to ray-tracing calculations for this case, the time it takes the wave to travel from the Earth to the spacecraft is ~ 0.24 s, based on the electron density profile shown in Figure 3a. As we can see in the spectrogram shown in Figure 4a, the calculation assumes that the whistler propagates in a duct. A second whistler is

also observed, reaching the spacecraft ~ 0.8 s later. According to its dispersion characteristics, this whistler is likely specular, a reflection of the original wave in the lower ionosphere at the conjugate point in the hemisphere opposite to that of the source. This reflected whistler travels back to the spacecraft from its reflection point, in the direction opposite to that of the initial whistler. However, careful examination of the time delays indicates that the reflected whistler does not propagate back to the spacecraft along the same path as the initial whistler. If such was the case, then the delay between the first whistler and the reflection should be ~ 0.5 s, while the data show a delay of ~ 1.2 s at the nose frequency of ~ 4.9 kHz. According to the dispersion characteristics and the regular repetitive occurrence of the reflected component, it is likely that this component is a reflection from the ionosphere of a whistler generated by the same lightning flash, which initially propagates to the hemisphere of reflection, at a different L shell. This assumption is verified with a ray-tracing simulation, using the electron density profile of Figure 3a, launching waves from the ionosphere at an L shell of 3.3, and magnetic latitude of 53° south, so that they can be guided by the inner boundary of the plasmopause [Inan and Bell, 1977]. Under

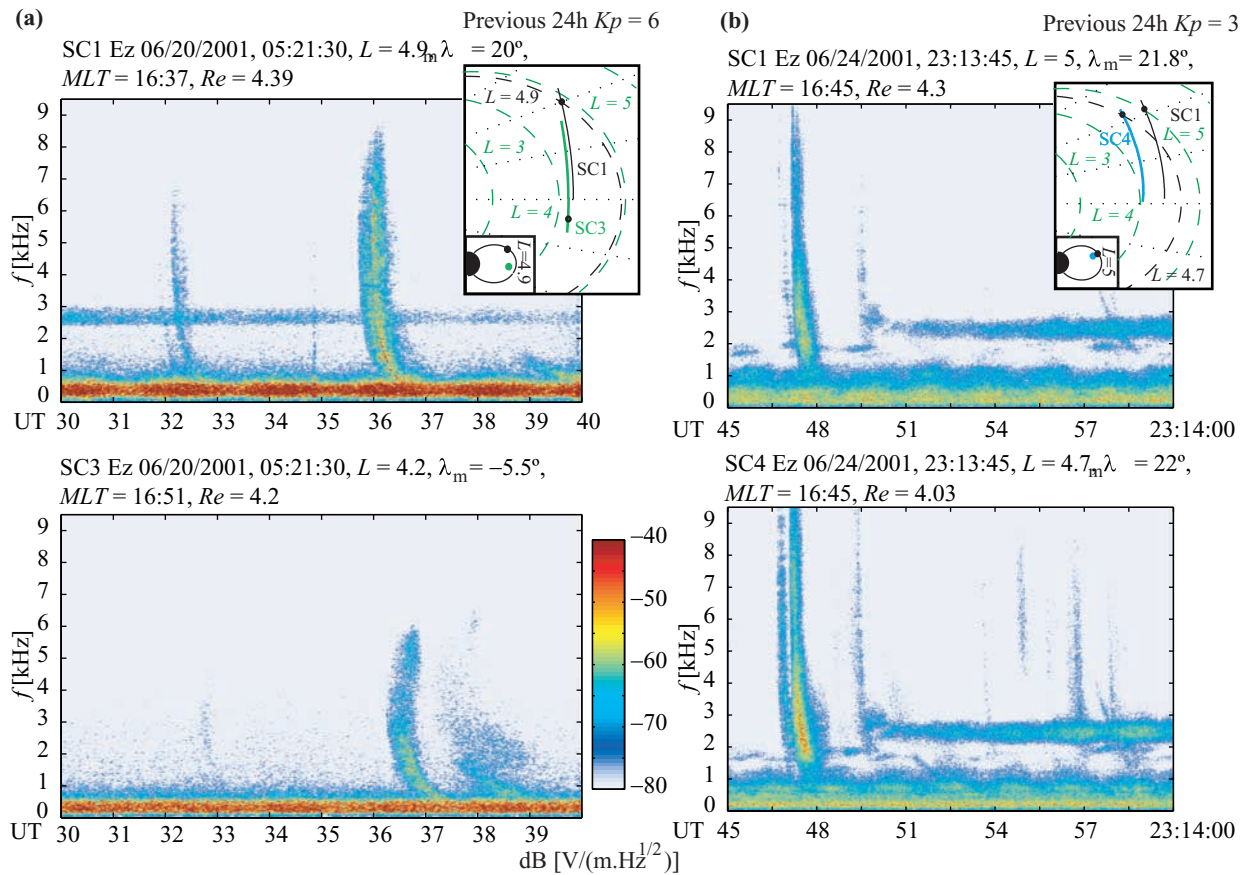


Figure 6. (a) WBD electric field spectrogram for 06/20/2001, when whistlers outside the plasmasphere were recorded. Displayed are time, location of the spacecraft, and geomagnetic activity index Kp . We find two whistlers detected on two different spacecraft, with different dispersion characteristics, due to the separation of spacecraft SC1 and SC3 in latitude. (b) WBD electric field spectrogram for 06/24/2001, when whistlers outside the plasmasphere were recorded. Displayed are time, location of the spacecraft, and geomagnetic activity index Kp . In this case, data were recorded on spacecraft SC1 and SC4, both being mostly separated in L shell.

this scenario, we see that the delay for the first hop from the Southern Hemisphere to the conjugate point in the Northern Hemisphere is ~ 1.29 s. The reflected wave travels back to SC3 following $L = 4$, reaching the spacecraft ~ 1.57 s after it was launched. The other whistler wave launched directly from the Southern Hemisphere travels toward SC3 and reaches the spacecraft after ~ 0.28 s. This gives us a delay between the direct path and the reflected one of ~ 1.29 s. All these ray paths are shown in Figure 4b, and the calculations were done for the nose frequency ($f = 4.9$ kHz). Results agree with the data (the measured delay between both waves is 1.2 s), corroborating the original assumption that the reflected components are in fact reflections from the ionosphere of whistlers that were originally guided by the plasmopause.

[25] The noise band that appears around the nose frequency appears to contain a number of triggered emissions. The amplitude of the noise band changes periodically with the spin rate of the spacecraft. This spin modulation is produced by the change of position of the electric antenna, with respect to the detected wave polarization. The local gyrofrequency in this case is 13.5 kHz. We also note here the upper cutoff of the whistler to be near half the equatorial

gyrofrequency (~ 6.7 kHz), which is the expected cutoff frequency for waves propagating in the whistler mode within a duct [Helliwell, 1965, p. 126].

[26] Figure 5a corresponds to data for 20 June 2001. This figure shows three whistler components, two of them separated by 0.2 s and the third one delayed by 2.4 s as observed on two different spacecraft. Since the L shells on which the two spacecraft are located are similar, it is reasonable to assume that the whistler waves were first observed on SC1 and they subsequently propagated to SC3. It is interesting to note that the dispersion of the whistlers changes significantly as the waves travel from spacecraft SC1 to spacecraft SC3. The gyrofrequency at spacecraft SC1 is around 12 kHz, while the gyrofrequency at spacecraft SC3 is around 12.5 kHz. The first two whistlers observed by SC1 have a cutoff of 8 kHz, which is ~ 2 kHz above the half gyrofrequency, while the third whistler cuts off at ~ 7 kHz, approximately 1 kHz above the half gyrofrequency. This difference might be related to the different intensities of the first two whistlers with respect to the third one, as well as deviations of the Earth's magnetic field from the centered dipole model. These three whistlers are seen again by spacecraft SC3, with a much

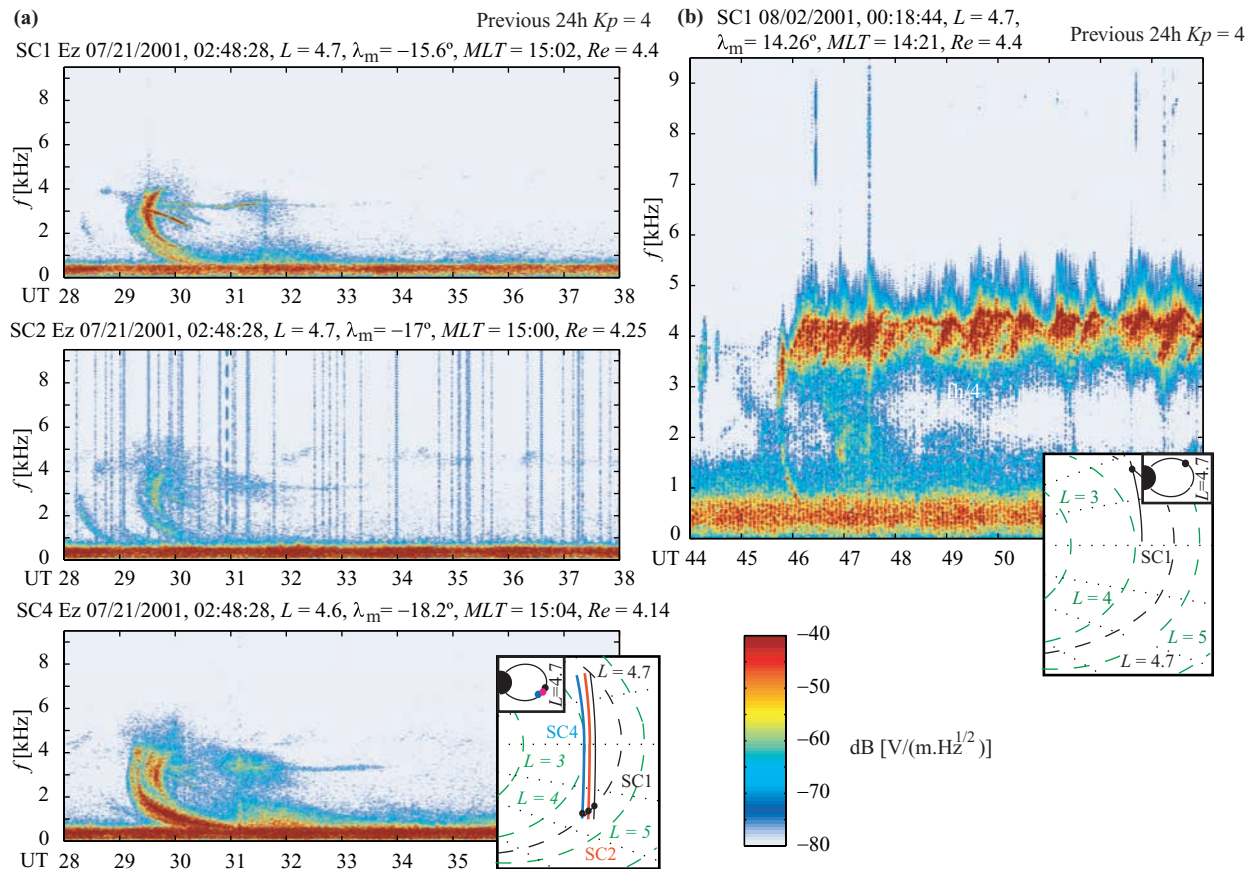


Figure 7. (a) WBD electric field spectrogram for 07/21/2001, when whistlers outside the plasmasphere were recorded. Displayed are time, location of the spacecraft, and geomagnetic activity index K_p . Here we have available data from SC1, SC2, and SC3 flying in a closer arrangement. The whistler shown has a very interesting structure that hints of a combination of different effects in one single case: propagation effects and triggered emissions. (b) WBD electric field spectrogram for 08/02/2001, when whistlers outside the plasmasphere were recorded. Displayed are time, location of the spacecraft, and geomagnetic activity index K_p . As in the case shown in Figure 4, this case has also a whistler and triggered emissions generated from it.

lower cutoff (~ 4 kHz) and delayed in time by 0.7 s with respect to their reception on SC1. Ray tracing in this case shows that rays with frequency below 3 kHz launched from the Northern Hemisphere at a latitude of 58.8° tend to deviate from L shell 4.7 toward lower L shells, after the magnetic equator, passing close to SC3 at $L = 4.3$, as can be seen in Figure 5b. The delay calculated for this case, between the whistler appearing in SC1 and the one in SC3 is 0.76 s at 3 kHz, which agrees with the measured delay of ~ 0.7 s.

[27] Figure 6a displays a case similar to that in Figure 5a showing two different whistlers, the first one weak and the second one strong. This data were acquired during the same pass as that shown in Figure 5, but 7 min later, at 0521:30 UT. The local gyrofrequency at the locations of both spacecraft SC1 and SC3 is around 12 kHz. It can be seen that the upper cutoff frequency for the strong whistler seen on SC3 is around half the gyrofrequency (~ 6 kHz), but the strong whistler at spacecraft SC1 exhibits a cutoff that is 2 kHz above the half gyrofrequency (~ 8 kHz).

[28] Figure 6b shows a whistler observed on 24 June 2001, at 2313:47 UT. The gyrofrequency at spacecraft SC1 is 13.2 kHz, while that at spacecraft SC4 is 16 kHz. Once again we notice that the whistler extends up to ~ 1.5 kHz above the half gyrofrequency. The spin modulation of the hiss intensity at lower frequencies is also evident. The VLF noise band that appears after the whistler at ~ 2.7 kHz is triggered by the wave, in a similar way as the one noted in Figure 4. We should mention though that this triggered noise band exhibits the characteristic of having a low intensity at the beginning, while increasing its intensity in time. This variation may be explained as a suppression of the VLF noise band produced by the whistler that triggered it, as was discussed by *Gail and Carpenter* [1984].

[29] Figure 7a shows a whistler event with interesting structure, recorded on 21 July 2001. As is shown below, the detailed dispersion structure is well reproduced by ray tracing, leading us to the conclusion that most of this structure is produced by propagation effects and is not due to triggering of emissions. It is important to notice also the difference in intensity of the wave at the different

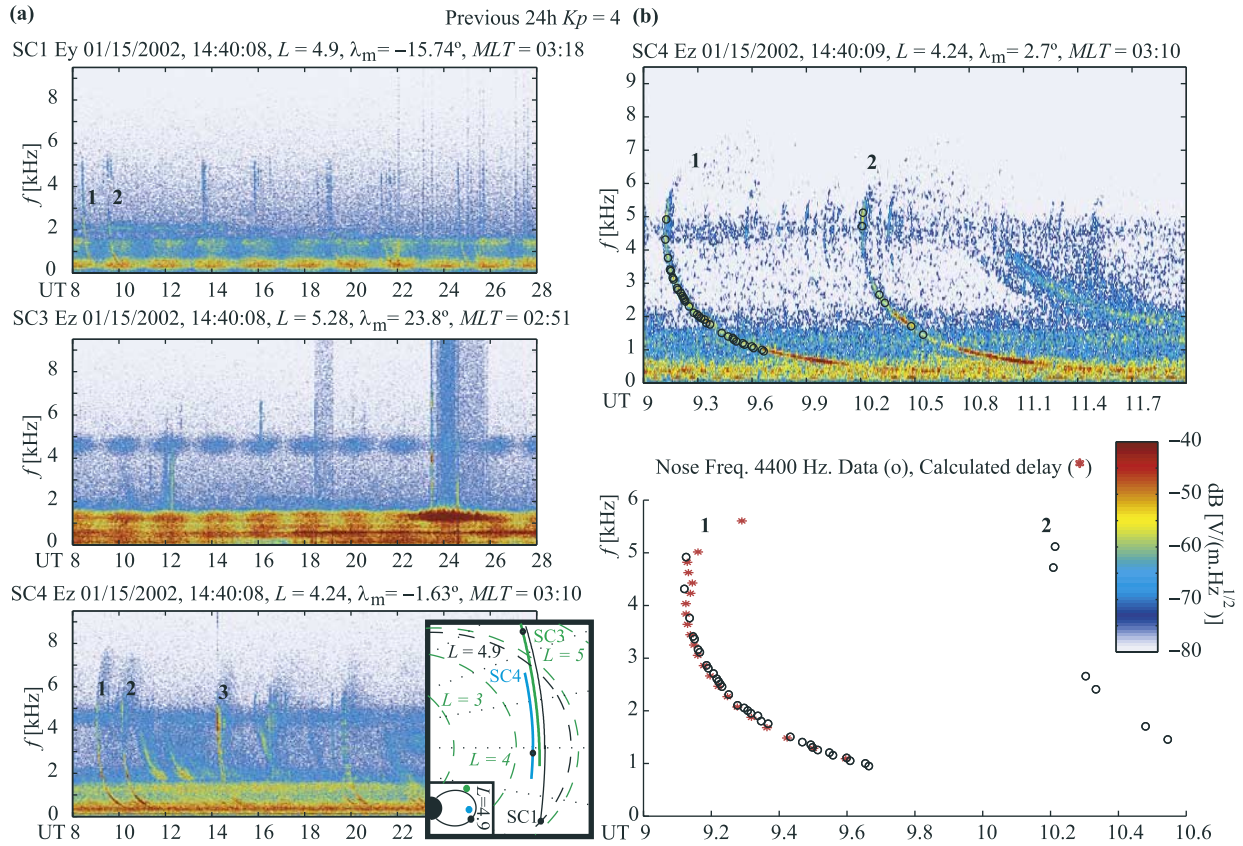


Figure 8. (a) WBD electric field spectrograms for 01/15/2002, when whistlers outside the plasmasphere were recorded. Each panel displays time, location of the spacecraft, and geomagnetic activity index K_p . There is a noticeable difference in the first and third spectrograms compared to the second spectrogram. This is due to the relative location of the spacecraft, SC1 and SC4 being closer to each other, while both were far away from SC3. (b) A comparison between the measured data (black circles) and the calculated delays (red asterisks), using ray tracing. This figure is a first-order approximation but uses the same principle of the calculation associated with Figures 13 to 16.

spacecraft, suggesting that the whistler in this case is confined to a narrow duct, with SC1 and SC4 crossing the duct at the time the whistler is observed on these spacecraft, while SC2 is the one positioned farther away from the duct and thus only sees wave energy that leaks out of the duct. This conclusion can be reached only if the intensity measured on the three spacecraft is calibrated to the same scale, in order for them to be compared. All the measurements shown in this paper using the WBD instrument with the electric antenna are calibrated in this fashion. The local gyrofrequency is 12.8 kHz, and at each of the three spacecraft the whistler spectra is observed below the half gyrofrequency point. Ray-tracing simulations show that waves between 5 and 6 kHz tend to deviate away from the field-aligned duct, which may account for the observed relatively low whistler cutoff at ~ 4.5 kHz.

[30] Figure 7b shows a whistler recorded on 2 August 2001 at 0018:45.6 UT. The distinctive characteristic of this whistler is that triggers a burst of VLF emissions that extend for about 30 s after the initial triggering. The local gyrofrequency for this case is 11.3 kHz. Emission bursts such as this one are known to be triggered by whistlers and have been observed on the ground [Dingle and Carpenter, 1981]. Similar emissions have been observed on the ground

[Helliwell and Katsufurakis, 1974] and in space [Inan et al., 1977], in active experiments performed using the Siple station in Antarctica. Evidence of triggered emission propagation outside the plasmasphere following plasma trough density gradients was reported by Carpenter and Miller [1983] based on observations made during experiments of injection of VLF waves into the magnetosphere using the Siple station at Antarctica, showing that ducted propagation of these emissions outside the plasmasphere is possible.

6. Data Recorded During 2002

[31] Figure 8a shows data recorded on 15 January 2002 at 1440:08 UT. These data show three different distinctive whistlers marked 1, 2, and 3 (and probably four more very weak ones), detected in spacecraft SC1 and SC4. Spacecraft SC3 shows data that do not appear to be correlated with the other two, possibly due to the fact that it is located too far away from them. The first two whistlers, detected at $\sim 1404:09$ UT at spacecraft SC4 and $\sim 1440:08.6$ UT at spacecraft SC1, are separated by ~ 1 s from each other. Ray-tracing calculations show that the time it takes for the wave to propagate from the Earth to the spacecraft is ~ 0.53 s. These rays have to originate in the Southern Hemisphere, in

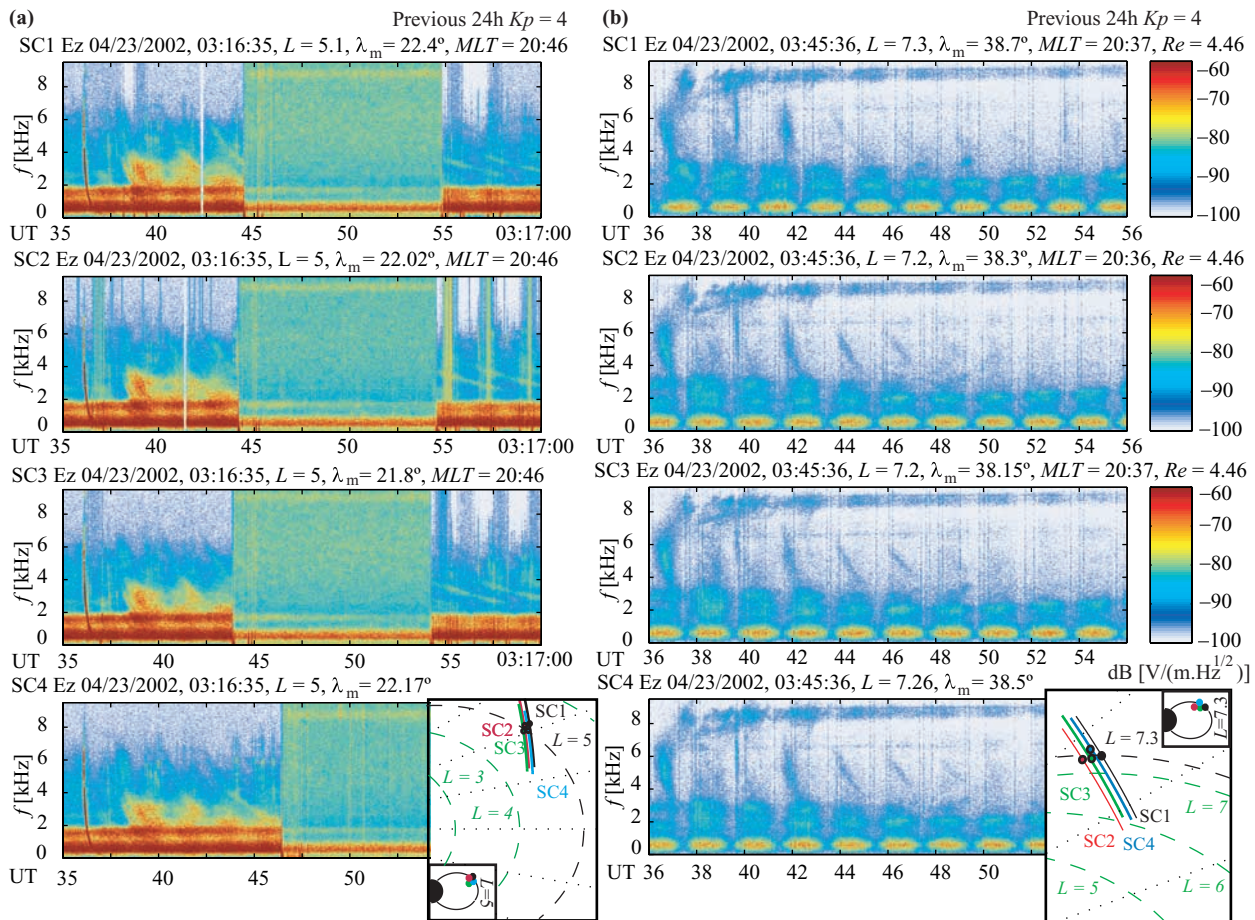


Figure 9. WBD electric field spectrograms for 04/23/2002, when whistlers outside the plasmasphere were recorded. Each panel displays time, location of the spacecraft, and geomagnetic activity index Kp . Reflections and triggered emissions were recorded on the four Cluster spacecraft for most of the whistlers. (a) We see a switch from the electric antenna E_z to the search-coil magnetic antenna B_y for a short period of 5 s. (b) There is a noticeable spacecraft spin fading modulation with a period of 2 s.

order to be detected first on SC1 and subsequently on SC4. The electron density profile used in this case for the ray-tracing calculation was based entirely on the *Carpenter and Anderson* [1992] model, with a local density enhancement of 80% placed at L shells 4.25 and 4.9. These should be considered to only be first-order calculations, since Whisper data were not used to build the density profile for this first approximation, and as we see from the results in Figure 8b, the match between ray-tracing calculations and data is fairly good. An interesting result from these calculations is the following:

[32] 1. A small shift of 2° in latitude of the position of the source in the ionosphere results in the waves being trapped either by the duct at $L = 4.25$ or at $L = 4.9$, indicating that the same lightning source may have generated both of the whistlers, with the wave energy propagating in the Earth-ionosphere waveguide leaking out into the magnetosphere at different latitudes. These two whistlers are the ones marked as 1 and 2, detected by SC1 at $L \sim 4.9$ and by SC4 at $L \sim 4.25$.

[33] 2. The reflected whistler seen at ~ 1.8 s later (most prominently visible on SC4) also fits well with the ray-tracing model predictions, as the time calculated for the

wave to travel from the ionosphere to the spacecraft is ~ 0.53 s, while the time it takes the wave to propagate from the spacecraft to the conjugate point and back is about 1.72 s.

[34] The nose frequency of the two whistlers observed by SC1 and SC4 (marked as 1 and 2) is 4.4 kHz. Figure 8b shows the results of the ray-tracing calculations done for these whistlers. This Figure is a simplified version of the calculations done in Figures 13 to 16, showing the correspondence between calculated time delays (shown in red asterisks) and the data (selected points from the actual whistlers are shown as black circles). This first approximation is primarily intended to simply show the kind of comparative analysis that is presented in more detail later.

[35] Figure 9a shows a whistler recorded on 23 April 2002 at 0316:35 UT. Following the whistler is a long train of multiple reflections with a repetition period of ~ 2.5 s at 3 kHz.

[36] The echoes following the first whistler have a period of ~ 3 s which remains constant in time as the spacecraft move, suggesting that the spacecraft are not located within the duct in which the whistler is propagating, considering that the duct is small enough to be crossed by the spacecraft

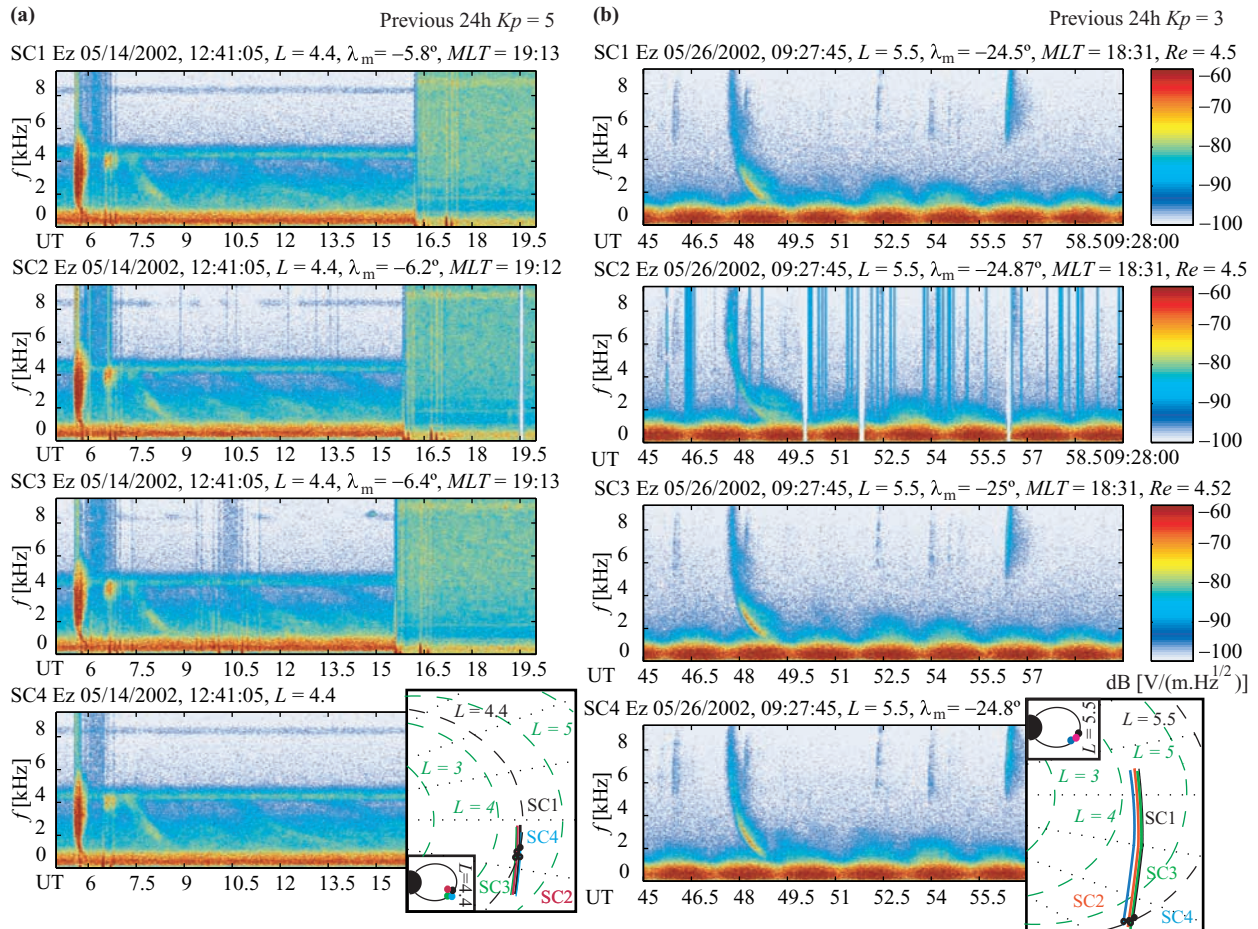


Figure 10. (a) WBD electric field spectrograms for 05/14/2002, when whistlers outside the plasmasphere were recorded. Each panel displays time, location of the spacecraft, and geomagnetic activity index Kp . Here we also find reflections of the whistler as well as the switch from the electric to the magnetic antenna. (b) WBD electric field spectrograms for 05/26/2002, when whistlers outside the plasmasphere were recorded. Each panel displays time, location of the spacecraft, and geomagnetic activity index Kp . We find the four spacecraft flying in close formation.

during the time we continue to see these reflections (which can last up to 1 min). The fraction of time when the amplitude changes suddenly corresponds to a switch of antennas, from the electric to the search-coil magnetic antenna. The local gyrofrequency at the time of acquisition of the data shown in this panel is ~ 12.8 kHz, and the frequency cutoff of this whistler is around the half gyrofrequency point (~ 6.5 kHz).

[37] Figure 9b shows a whistler recorded during the same pass as that shown in Figure 9a, but half an hour later, at 0345:36 UT. In this case we once again see a whistler and its multiple reflections. This whistler also triggers emissions above the cutoff frequency of the whistler. The spin modulation is also clearly evident. The local gyrofrequency is 14.7 kHz, and the whistler cutoff frequency is around the half gyrofrequency (~ 7.3 kHz).

[38] Figure 10a shows a whistler and its reflection for 14 May 2002. Once again, we notice the shift in intensity, corresponding to the switching of antennas, from the electric to the search-coil magnetic antenna. The reflection in this case appears with a delay of 1.5 s at 3 kHz after the whistler itself. The whistler nose frequency is

4.1 kHz and the local gyrofrequency is 11.3 kHz. The cutoff frequency of the whistler is at the half gyrofrequency (~ 5.7 kHz).

[39] Figure 10b shows a whistler detected on 26 May 2002 at 0927:47 UT. In this case, the spin modulation is evident at low frequencies and there are noticeable differences in intensity among the waves detected by spacecraft SC1, SC3, SC4, and those detected by SC2. As we saw in the 21 July 2001 case, the difference in intensity between spacecraft can be explained as being due to their different positions with respect to the duct, within which the whistler propagates. It should also be noted that the different antennas in each spacecraft are oriented in different directions with respect to the whistler wave fronts.

[40] Figure 11 shows three different whistlers recorded on 26 May 2002 at 0947:05 UT. Here we notice an important difference in intensity between the spectra above and below 3 kHz. This effect may be produced by amplification of the lower frequencies within a duct, consistent with the fact that this is a very active day in terms of detected whistlers.

[41] Figure 12 shows a projection on the meridional (Figure 12a) and equatorial (Figure 12b) plane of the

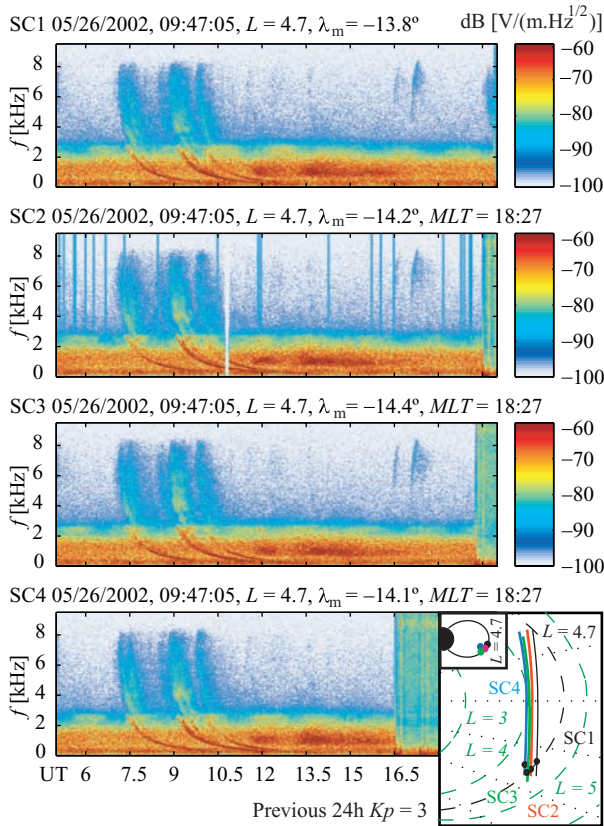


Figure 11. WBD electric field spectrograms for 05/26/2002, when whistlers outside the plasmasphere were recorded. Each panel displays time, location of the spacecraft, and geomagnetic activity index Kp . Again, we find the four spacecraft flying in close formation.

Cluster orbital segments during which data were acquired for the present study. The results shown indicate that the whistlers are predominantly observed in the afternoon sector of 1400–2400 MLT, although there also exists a case of observations in the early morning sector, around 0300 MLT. The L shell range of observations is limited to 4–5. Shown are the 10 orbit passes discussed in this paper, on which whistlers outside the plasmasphere were detected with the Cluster WBD instrument during 2001 and 2002. Of the 10 passes, nine occur in the afternoon sector.

7. Simulation Results

[42] The results of our ray-tracing analyses are shown in Figures 13, 14, 15, and 16. Each figure describes the simulation results and the data for comparison purposes. The computed intensities displayed were estimated using a simple ray counting technique. This technique consists of launching a dense number of rays (~ 400 rays for each case) in order to be able to count the number of rays in a close region around the spacecraft of $10 \text{ km} \times 10 \text{ km}$. Depending on the values of Δf and Δt used for each pixel in the reconstructed whistler, the number of rays with delay and frequency within that pixel were added up to obtain the amplitude value displayed. This method is repeated for each frequency-time pixel and the simulated whistler spectrogram is then constructed as follows: For every pixel, the rays that reach the spacecraft, at the frequency and time corresponding to that pixel are counted. The displayed color of the pixel is then selected according to the scale shown to the right, increasing the intensity as the number of rays for that pixel increases. The scale shown in Figures 13 to 16 has an arbitrary level set to 1 ray counted for light blue (-30 dB) to 10 rays counted for red (0 dB). The ray-tracing results are in good agreement with the measured signal spectra, for cases

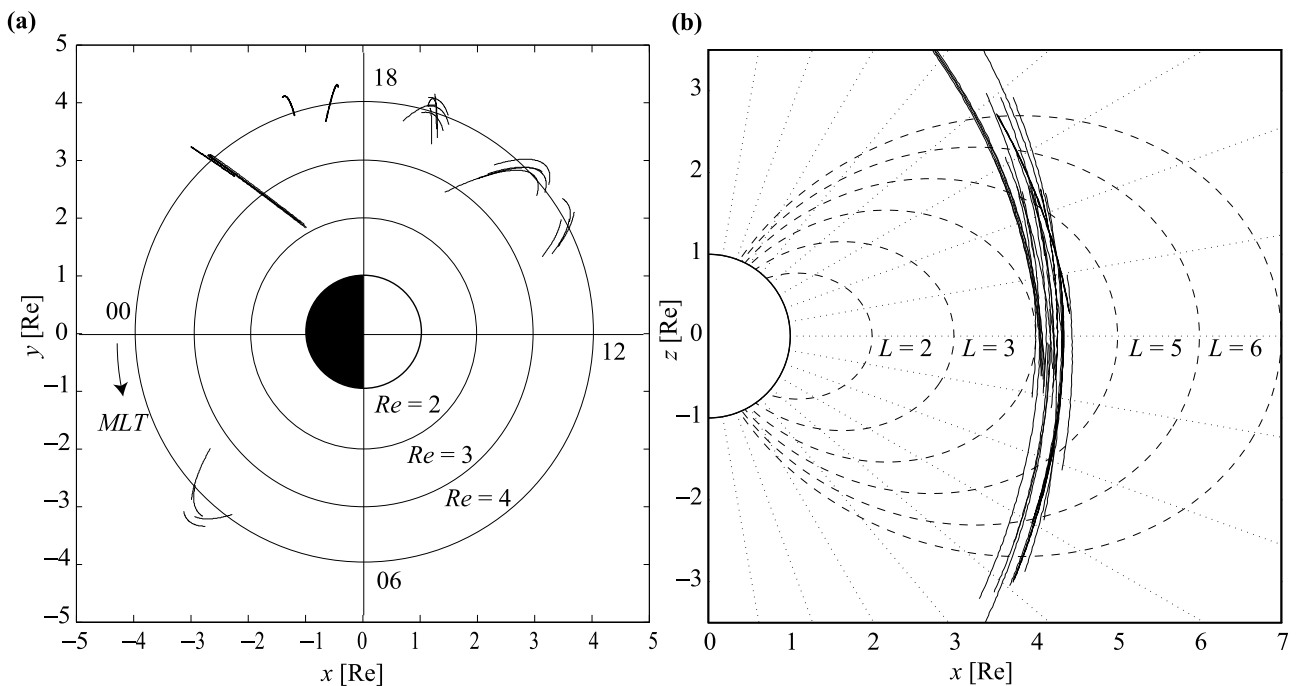


Figure 12. (a) Meridional and (b) equatorial projection of Cluster orbits during which whistlers observed in Figures 4 to 11 were recorded during 2001–2002.

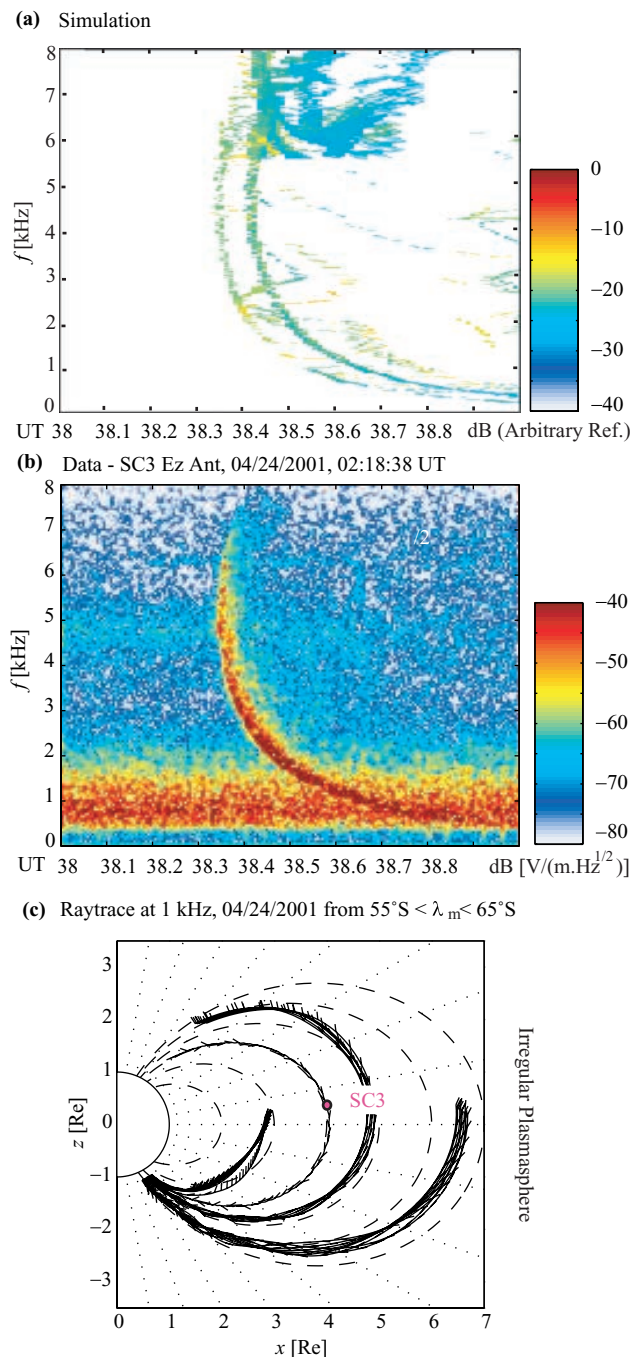


Figure 13. Simulation results for 24 April 2001, 02:18:38 UT. (a) Simulated whistler using ray tracing. The amplitude scale in this spectrogram has an arbitrary reference, since each pixel color was determined based on ray counting. (b) WBD measured electric field spectrogram. (c) Ray paths from the simulation, for rays launched at 1 kHz from different latitudes on the ground, are shown to display typical ray paths. Lower-frequency rays tend to curve toward lower L shells, while higher-frequency rays move toward higher L shells. If the rays are ducted, all the rays tend to stay within the duct in the frequency range shown in the spectrogram.

where the plasmaspheric electron density is highly irregular. Such is the case in Figure 16, for 07/21/2001.

[43] In the other cases, the agreement between data and calculation is not as good, depending on the smoothness of the plasmasphere and the intensity of the lightning strike that caused the whistler.

[44] Figure 13 shows the results for the 24 April 2001 case, showing good agreement with the measured data, but the ray-tracing results show two whistlers instead of one, the second one being 20 dB weaker than the first one on average. This propagation effect is not evident in the data, even though we would probably not be able to see the weaker whistler because of background noise. If we repeat the ray tracing for the same case but use only one duct located around $L = 4$, we find that the time delay estimated from this calculation at the nose frequency of the whistler (4.9 kHz) is 0.27 s. Comparing to the results of the calculations shown in Table 1, we conclude that for this case, wave propagation occurs within this single duct. We should also mention that the structure that ray-tracing results show above 5.5 kHz also corresponds to very low intensities, which probably represent calculation error due to paucity of rays.

[45] Figure 14 shows the results of ray tracing performed for the case of 20 June 2001 at 05:14:09 UT, showing not as good agreement with the measured data, especially in terms of the dispersion seen in the measurements. This result shows that such dispersion is probably not caused by propagation effects but is rather due to wave mode conversion produced by irregularities in the plasma density [Bell and Ngo, 1990]. This physical linear-mode conversion process was recently observed to occur outside the plasmasphere during an experiment performed with the HAARP ionospheric heater in Gakona, Alaska, injecting ELF/VLF signals by modulating ionospheric electrojet currents that were detected by the Cluster spacecraft [Platino *et al.*, 2004]. Whistler mode wave energy is apparently converted into lower hybrid waves modes [Bell *et al.*, 2004] due to refraction in irregularities in plasma electron density. This process can occur multiple times with whistler mode waves that convert to lower hybrid mode waves and back to whistler mode waves, in the presence of highly irregular plasma density distributions, such as the ones in 20 June 2001 and 21 July 2001. During this multiple-conversion process the group velocity of the wave changes, leading to the dispersed and smeared characteristic of the whistler, as seen in Figures 13 to 16. The end result is a whistler being dispersed during a long time such as the one seen in Figure 14 (~ 0.8 s). Particularly in Figure 14, we see four clearly distinctive whistlers with the later one being the strongest one, as the highest response to the electric antenna of the Cluster spacecraft is achieved with lower hybrid mode waves. Mode conversion effects do not occur in case of smoother plasma density distribution as the one on 24 April 2001, and the whistlers measured during that day do not exhibit this dispersed and smeared characteristic. If we repeat the ray tracing for the 24 April 2001 case but use only one duct located at $L = 4.7$, we find that the time delay estimated from this calculation, at the nose frequency of the whistler (4.7 kHz) is 0.27 s. Comparing with the results of calculations shown in Table 1, we conclude that for this case, propagation happens in this single duct. The same conditions probably exist in the next case, as is evident from Figure 15, where we are once again unable to reproduce the dispersion

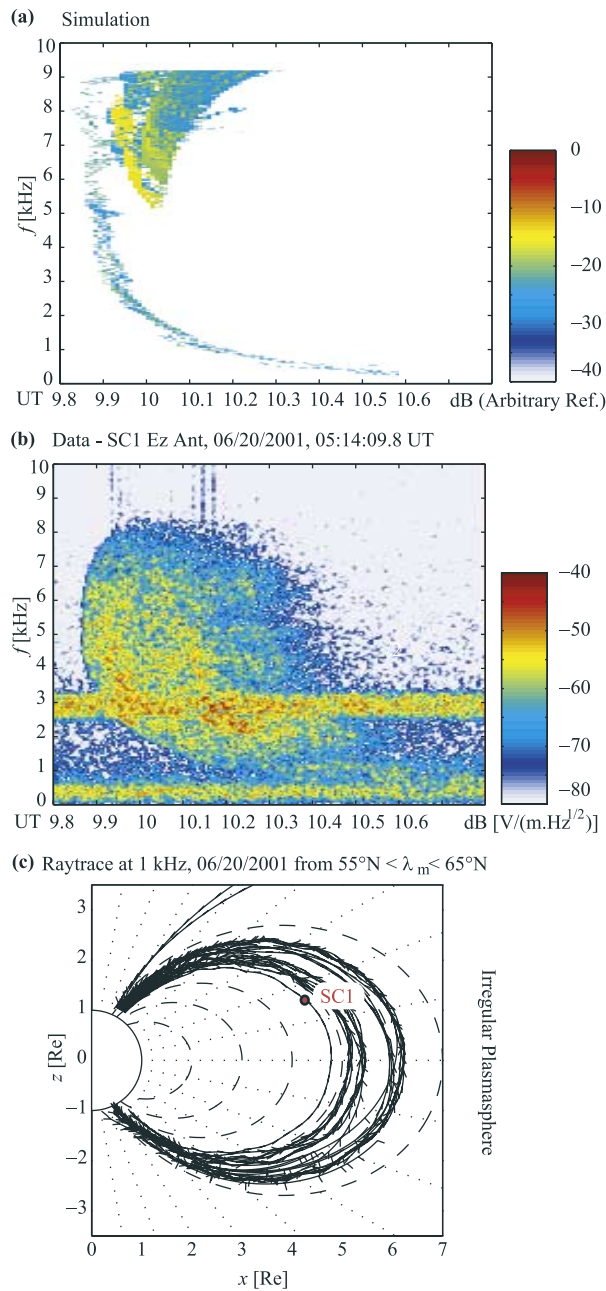


Figure 14. Simulation results for 20 June 2001, 0514:09.9 UT. (a) Simulated whistler using ray tracing. The amplitude scale in this spectrogram has an arbitrary reference, since each pixel color was determined based on ray counting. (b) WBD measured electric field spectrogram. (c) Ray paths from the simulation, for rays launched at 1 kHz from different latitudes on the ground, are shown to display typical ray paths. Lower-frequency rays tend to curve toward lower L shells, while higher-frequency rays move toward higher L shells. If the rays are ducted, all the rays tend to stay within the duct in the frequency range shown in the spectrogram.

evident in the data. The ray tracing using only one duct at the corresponding L shell ($L = 4.9$) yields a propagation time from the Earth to the spacecraft of 0.27 s. Once again, this calculated time is similar to that obtained from the calcula-

tions in Table 1, suggesting that for this case the whistler propagates in one single duct.

[46] Figure 16 represents the most interesting case. Here we see that the ray-tracing results closely resemble the measured whistler, even in terms of the fine structure. Ray-tracing calculations using only one duct at the L shell of the spacecraft ($L = 4.7$) results in a propagation time of 0.34 s, which differs significantly from that calculated using the entire profile as measured by the Whisper instrument, as specified in Table 1 ($t_m = 0.75$ s). This difference leads us to conclude that this particular case is showing an important influence of propagation effects, which dominate the structure we see in dispersion of the measured data. This means that the propagation of the whistler cannot be considered as the guiding within one single duct but the combination of guiding within several ducted paths within the trajectory, a case that can only happen if the plasma density is highly irregular as we see in this day.

8. Conclusions

[47] The ray-tracing technique shows good agreement with data, especially for days such as 07/21/01 (Figure 16), when the electron density outside the plasmasphere is very irregular. Cases like these are the ones for which we can accurately reproduce the fine structure of the whistler. This leads to the conclusion that these kinds of structures in whistlers are a sign of how irregular the electron density can be.

[48] The study of the cases on 06/20/01 and 04/24/01 provided more evidence to sustain this conclusion. Especially on 04/24/01 (Figure 13), we see that the detected whistler particularly propagates in a duct, and matches the simulation in a close manner. The two cases on 06/20/01 (Figures 14 and 15) correspond to a smoother density profile, where the irregularities are not so sharp. For this case the ray tracing is showing a similar signature in frequency, but the dispersion of the signal in time is not matched. The new results presented in this paper show that in all cases studied, whistlers were detected in the presence of ducts. This suggests that the presence of ducts is a necessary condition to detect whistlers outside the plasmasphere. Refer to Table 1 for the calculated location of the ducts for the cases studied.

[49] This conclusion is sustained with the limited statistics we have for the cases shown in this paper. All the whistlers detected on the days shown here are seen outside the plasmasphere.

[50] This study supports the idea that whistlers can be detected only sporadically outside the magnetosphere. We suggest that the general lack of whistlers in this region of the magnetosphere is likely due to mode conversion of electromagnetic whistler mode waves to quasi-electrostatic lower hybrid mode waves. These waves then propagate from the region f excitation, dissipating the energy of the electromagnetic whistler mode waves [Bell and Ngo, 1990]. This process of mode conversion between whistler and lower hybrid modes was reproduced in a laboratory experiment and reported [Bamber et al., 1994]. In this experiment, the lower hybrid waves had amplitudes up to 20% of the incident whistler waves; this means that 4% of the whistler mode energy was transformed into lower hybrid, while the rest of the energy was retained in the reflected whistler mode waves, the transmitted lower hybrid waves,

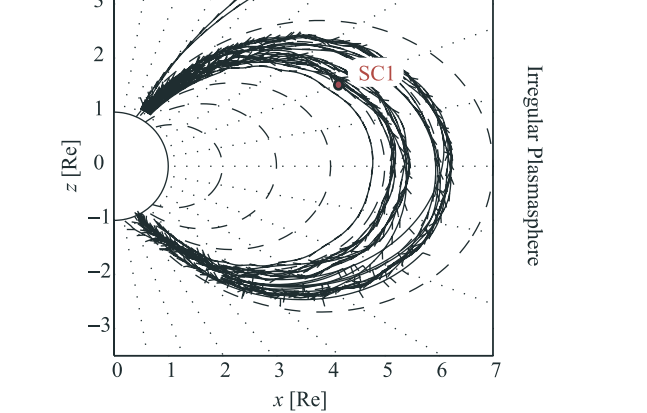
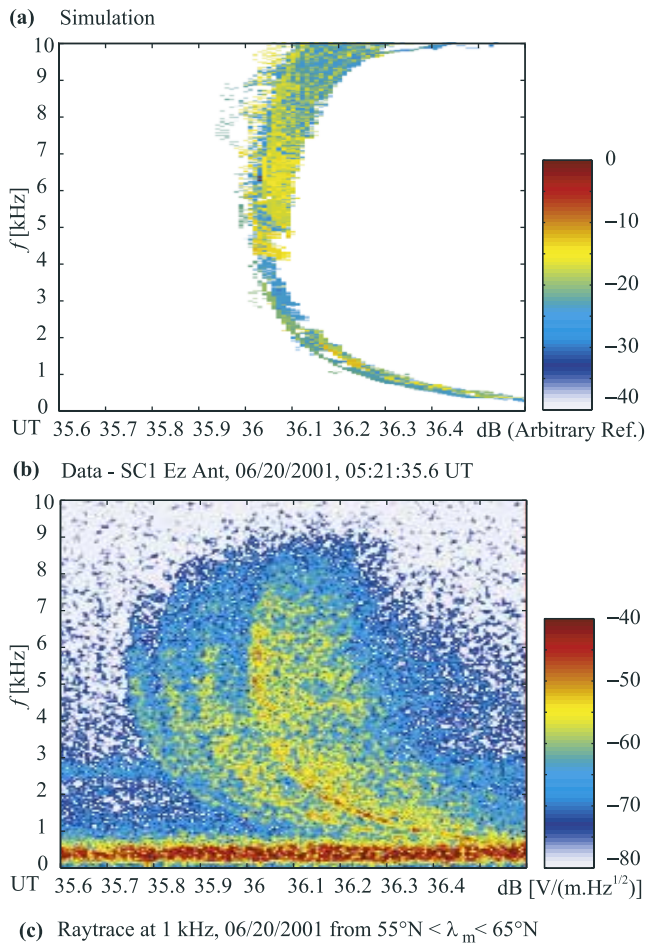


Figure 15. Simulation results for 20 June 2001, 0521:35.6 UT. (a) Simulated whistler using ray tracing. The amplitude scale in this spectrogram has an arbitrary reference, since each pixel color was determined based on ray counting. (b) WBD measured electric field spectrogram. (c) Ray paths from the simulation, for rays launched at 1 kHz from different latitudes on the ground, are shown to display typical ray paths. Lower-frequency rays tend to curve toward lower L shells, while higher-frequency rays move toward higher L shells. If the rays are ducted, all the rays tend to stay within the duct in the frequency range shown in the spectrogram.

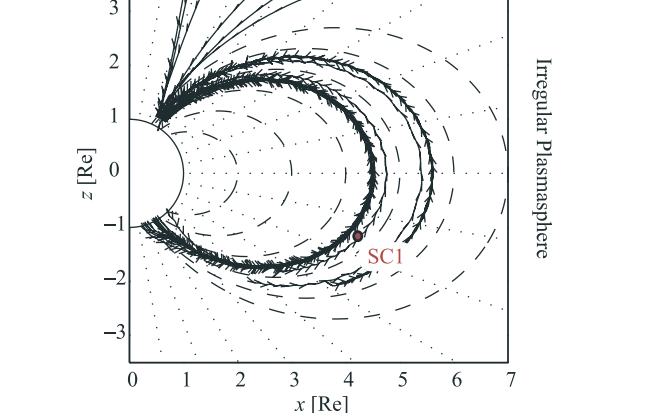
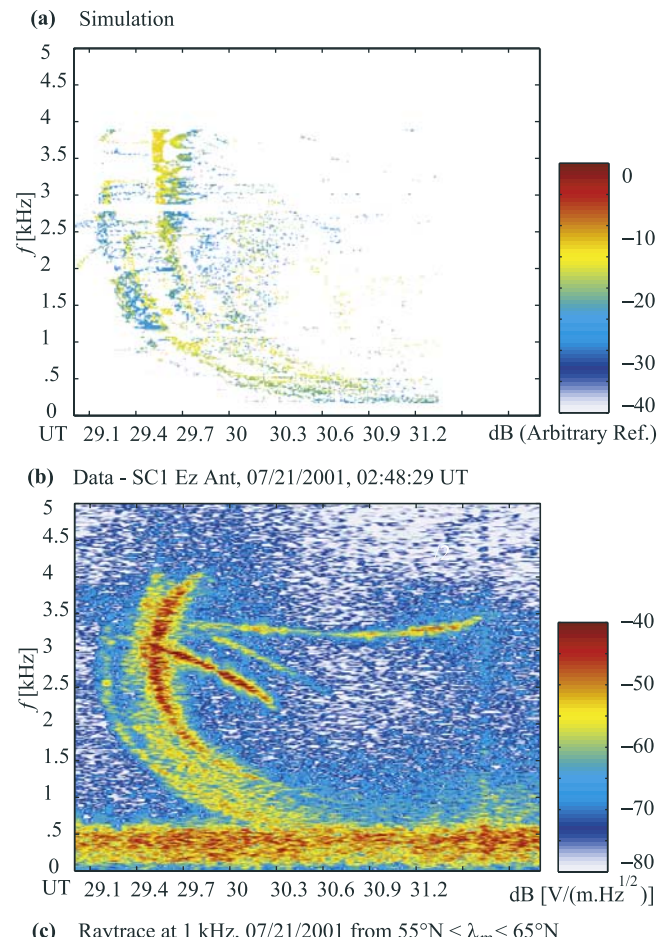


Figure 16. Simulation results for 21 July 2001, 0248:29 UT. (a) Simulated whistler using ray tracing. The amplitude scale in this spectrogram has an arbitrary reference, since each pixel color was determined based on ray counting. (b) WBD measured electric field spectrogram. (c) Ray paths from the simulation, for rays launched at 1 kHz from different latitudes on the ground, are shown to display typical ray paths. Lower-frequency rays tend to curve toward lower L shells, while higher-frequency rays move toward higher L shells. If the rays are ducted, all the rays tend to stay within the duct in the frequency range shown in the spectrogram.

and the whistler radiation that refracts around the irregularity. The HAARP-Cluster experiment studied by *Bell et al.* [2004] showed that the electric field amplitude of the lower hybrid waves was higher than that of the input whistler mode waves. According to *Bell and Ngo* [1990] and *Bamber et al.* [1994], if all of the whistler mode energy is converted to lower hybrid waves, then the lower hybrid energy density would be much higher than that of the whistler mode because the group velocity of lower hybrid waves is much slower than the one for whistler mode waves. This result agrees with the fact that most of the energy detected by the Cluster spacecraft and reported by *Bell et al.* [2004] and *Platino et al.* [2004] is lower hybrid. An interesting new conclusion presented in this paper is that as we see in the 20 June 2001 case, this mode conversion between whistler and lower hybrid modes can occur several times in the course of propagation of the wave along its path, sometimes leading to highly dispersed whistlers that last for almost a second or even more. The ray-tracing calculations show that for this case, this feature of the wave cannot be explained by wave propagation effects as specular reflections at the ionospheric end points of irregularities, since the dispersion characteristics do not match so well (see Figures 14 and 15).

[51] In general, our observations of whistlers outside the magnetosphere measured by the WBD instrument at the Cluster spacecraft (displayed in Figures 4 to 11) suggest that mode conversion from electromagnetic to quasi-electrostatic waves can be an important factor that explains the lack of whistlers outside the plasmasphere and the lack of whistler mode energy in general in this same region of space.

[52] **Acknowledgments.** This research was supported by the National Aeronautics and Space Administration, under parent grant NAG5-9974 at the University of Iowa, and with subcontract 4000061641 to Stanford University. We greatly appreciate the help of C. Abramo in scheduling the real-time wideband data acquisition from the WBD receiver at DSN and also the help of I. Christopher, J. Dowell, and J. Seeberger in reducing the data to usable form.

[53] Lou-Chuang Lee thanks the reviewer for the assistance in evaluating this paper.

References

- Angerami, J. J. (1966), A whistler study of the distribution of thermal electrons in the magnetosphere, *Tech. Rep. 3412-7*, Radiosci. Lab., Stanford Electr. Lab., Stanford Univ., Stanford, Calif.
- Angerami, J. J. (1970), Whistler duct properties deduced from VLF observations made with the Ogo 3 satellite near the magnetic equator, *J. Geophys. Res.*, *75*(31), 6115–6135.
- Angerami, J. J., and D. L. Carpenter (1966), Whistler studies of the plasmapause in the magnetosphere: 2. Electron density and total tube content near the knee in magnetospheric ionization, *J. Geophys. Res.*, *71*(3), 711–725.
- Bamber, J. F., W. Gekelman, and J. E. Maggs (1994), Whistler wave mode conversion to lower hybrid waves at a density striation, *Phys. Rev. Lett.*, *73*(22), 2990–2993.
- Bell, T. F., and H. D. Ngo (1990), Electrostatic lower hybrid waves excited by electromagnetic whistler mode waves scattering from planar magnetic-field-aligned plasma density irregularities, *J. Geophys. Res.*, *95*(A1), 149–172.
- Bell, T. F., U. S. Inan, M. Platino, P. A. Kossey, and E. J. Kennedy (2004), Cluster observations of lower hybrid waves excited at high altitudes by electromagnetic whistler mode signals from the HAARP facility, *Geophys. Res. Lett.*, *31*(6), L06811, doi:10.1029/2003GL018855.
- Bernstein, I. B. (1958), Waves in a plasma in a magnetic field, *Phys. Rev.*, *109*(1), 10–21.
- Canu, P., et al. (2001), Identification of natural plasma emissions observed close to the plasmapause by the Cluster-Whisper relaxation sounder, *Ann. Geophys.*, *19*(10–12), 1697–1709.
- Carpenter, D. L. (1978), Whistlers and VLF noises propagating just outside the plasmasphere, *J. Geophys. Res.*, *83*(A1), 45–56.
- Carpenter, D. L., and R. R. Anderson (1992), An ISEE/Whistler model of equatorial electron density in the magnetosphere, *J. Geophys. Res.*, *97*(A2), 1097–1108.
- Carpenter, D. L., and T. R. Miller (1983), Rare ground-based observations of Siple VLF transmitter signals outside the plasmapause, *J. Geophys. Res.*, *88*(A12), 10,227–10,232.
- Carpenter, D. L., and D. M. Sulić (1988), Ducted whistler propagation outside the plasmapause, *J. Geophys. Res.*, *93*(A9), 9731–9742.
- Carpenter, D. L., F. Walter, R. E. Barrington, and D. J. McEwen (1968), Alouette 1 and 2 observations of abrupt changes in whistler rate and of VLF noise variations at the plasmapause: A satellite-ground study, *J. Geophys. Res.*, *73*(9), 2929–2940.
- Carpenter, D. L., C. G. Park, H. A. Taylor Jr., and H. C. Brinton (1969), Multiexperiment detection of the plasmapause from EOGO satellites and Antarctic ground stations, *J. Geophys. Res.*, *74*(7), 1837–1847.
- Cerisier, J. C. (1967), Accessibility by propagation of very low frequency resonances in the ionosphere, *Ann. Geophys.*, *23*(2), 249–266.
- Décrou, P. M. E., et al. (1997), Whisper, a resonance sounder and wave analyzer: Performances and perspectives for the Cluster mission, *Space Sci. Rev.*, *79*(1–2), 157–193.
- Dingle, B., and D. L. Carpenter (1981), Electron precipitation induced by VLF noise bursts at the plasmapause and detected at conjugate ground stations, *J. Geophys. Res.*, *86*(A6), 4597–4606.
- Etcheto, J., G. Belmont, P. Canu, and J. G. Trotignon (1983), Active sounder experiments on GEOS and ISEE, *ESA SP, 195*, 39–46.
- Gail, W. B., and D. L. Carpenter (1984), Whistler induced suppression of VLF noise, *J. Geophys. Res.*, *89*(A2), 1015–1022.
- Gurnett, D. A., R. L. Huff, and D. L. Kirchner (1997), The Wide-Band Plasma Wave investigation, *Space Sci.*, *79*(1–2), 195–208.
- Haselgrove, J. (1954), Ray theory and a new method for ray tracing, in *Report of Physical Society Conference on Physics of the Ionosphere*, pp. 355–364, Cambridge Univ. Press, New York.
- Helliwell, R. A. (1965), *Whistlers and Related Ionospheric Phenomena*, Stanford Univ. Press, Stanford, Calif.
- Helliwell, R. A., and J. P. Katsufakis (1974), VLF wave injection into the magnetosphere from Siple Station, Antarctica, *J. Geophys. Res.*, *79*(16), 2511–2518.
- Inan, U. S., and T. F. Bell (1977), The plasmapause as a VLF wave guide, *J. Geophys. Res.*, *82*(19), 2819–2827.
- Inan, U. S., T. F. Bell, D. L. Carpenter, and R. R. Anderson (1977), Explorer 45 and Imp 6 observations in the magnetosphere of injected waves from the Siple Station VLF transmitter, *J. Geophys. Res.*, *82*(7), 1177–1187.
- Kimura, I. (1966), Effects of ions on whistler-mode ray tracing, *Radio Sci.*, *1*(3), 269–283.
- Park, C. G. (1972), Methods of determining electron concentrations in the magnetosphere from nose whistlers, *Tech. Rep. 3454-1*, Radiosci. Lab., Stanford Electr. Lab., Stanford Univ., Stanford, Calif.
- Platino, M., U. S. Inan, T. F. Bell, J. Pickett, E. J. Kennedy, J. G. Trotignon, J. L. Rauch, and P. Canu (2004), Cluster observations of ELF/VLF signals generated by modulated heating of the lower ionosphere with the HAARP HF transmitter, *Ann. Geophys.*, *22*(7), 2643–2653.
- Smith, R. L. (1961), Propagation characteristics of whistlers trapped in field aligned columns of enhanced ionization, *J. Geophys. Res.*, *66*(11), 3699–3707.
- Trotignon, J. G., J. Etcheto, and J. P. Thouvenin (1986), Automatic determination of the electron density measured by the relaxation sounder on-board ISEE 1, *J. Geophys. Res.*, *91*(A4), 4302–4320.
- Trotignon, J. G., et al. (2001), How to determine the thermal electron density and the magnetic field strength from the Cluster/Whisper observations around the Earth, *Ann. Geophys.*, *19*(10–12), 1711–1720.
- Yabroff, I. (1961), Computation of whistler ray paths, *J. Res.*, *65D*(5), 485–505.

T. F. Bell, U. S. Inan, and M. Platino, STAR Laboratory, Stanford University, Stanford, CA 94305, USA. (platino@stanford.edu)

P. Canu, Centre d'Etudes des Environnements Terrestres et Planétaires, Centre National de la Recherche Scientifique, Université Versailles Saint-Quentin-en-Yvelines, 10 avenue de l'Europe, F-78140, Vélizy Villacoublay, France.

P. M. E. Décrou, Laboratoire de Physique et Chimie de l'Environnement, Centre National de la Recherche Scientifique, 3 A avenue de la Recherche Scientifique, F-45071 Orléans cedex 02, France.

D. A. Gurnett and J. S. Pickett, Department of Physics and Astronomy, University of Iowa, Iowa City, IA 52242, USA.